Published in final edited form as:
J Comp Neurol. 2007 February 10; 500(5): 876–893. doi:10.1002/cne.21207.

Selective Loss of Dentate Hilar Interneurons Contributes to Reduced Synaptic Inhibition of Granule Cells in an Electrical Stimulation-Based Animal Model of Temporal Lobe Epilepsy

CHENGSAN SUN[1], **ZAKARIA MTCHEDLISHVILI**[1], **EDWARD H. BERTRAM**[1], **ALEV ERISIR**[2], and **JAIDEEP KAPUR**[1,*]

[1] Department of Neurology, University of Virginia, Health Sciences Center, Charlottesville, Virginia 22908

[2] Department of Psychology, University of Virginia, Charlottesville, Virginia 22904

Abstract

Neuropeptide-containing hippocampal interneurons and dentate granule cell inhibition were investigated at different periods following electrical stimulation-induced, self-sustaining status epilepticus (SE) in rats. Immunohistochemistry for somatostatin (SOM), neuropeptide Y (NPY), parvalbumin (PV), cholecystokinin (CCK), and Fluoro-Jade B was performed on sections from hippocampus contralateral to the stimulated side and studied by confocal laser scanning microscopy. Compared to paired age-matched control animals, there were fewer SOM and NPY-immunoreactive (IR) interneurons in the hilus of the dentate gyrus in animals with epilepsy (40 – 60 days after SE), and 1, 3, and 7 days following SE. In the hilus of animals that had recently undergone SE, some SOM-IR and NPY-IR interneurons also stained for Fluoro-Jade B. Furthermore, there was electron microscopic evidence of the degeneration of SOM-IR interneurons following SE. In contrast, the number of CCK and PV-IR basket cells in epileptic animals was similar to that in controls, although it was transiently diminished following SE; there was no evidence of degeneration of CCK or PV-IR interneurons. Patch-clamp recordings revealed a diminished frequency of inhibitory postsynaptic currents in dentate granule cells (DGCs) recorded from epileptic animals and animals that had recently undergone SE compared with controls. These results confirm the selective vulnerability of a particular subset of dentate hilar interneurons after prolonged SE. This loss may contribute to the reduced GABAergic synaptic inhibition of granule cells in epileptic animals.

Indexing terms

somatostatin; neuropeptide Y; colocalization; status epilepticus

Temporal lobe epilepsy (TLE) is a common form of acquired medically refractory partial epilepsy. The pathogenesis of TLE has been investigated intensively by human studies and animal models, which have provided several explanations for the increased excitability of neurons in the epileptic hippocampus. These potential mechanisms include sprouting of new axon collaterals resulting in the formation of recurrent excitatory connections on granule cells, changes in the intrinsic excitability of neurons (McNamara, 1999), and the altered expression of neurotransmitter receptors, such as NMDA and $GABA_A$ receptors (Coulter, 2001).

*Correspondence to: Jaideep Kapur, MD, PhD, Department of Neurology, Box 800394, University of Virginia-HSC, Charlottesville, VA 22908. jk8t@virginia.edu.

One controversial and intensely investigated pathogenic mechanism is altered GABA-mediated inhibition. Neuroanatomical studies in human surgical specimens and experimental animal models of TLE have demonstrated a loss of inhibitory interneurons in the hilus of the dentate gyrus of the hippocampus (de Lanerolle et al., 1989; Sloviter, 1991; Obenaus et al., 1993; Mathern et al., 1995; Houser and Esclapez, 1996; Kobayashi and Buckmaster, 2003). These neuroanatomical studies are supported by electrophysiological studies demonstrating diminished paired pulse inhibition of CA1 pyramidal neurons and dentate granule cells (DGCs) (Kapur et al., 1989; Lothman et al., 1990; Sloviter, 1991; Sayin et al., 2003). A study of inhibitory synaptic transmission of DGCs of animals with TLE also demonstrated reduced frequency of inhibitory currents (Kobayashi and Buckmaster, 2003).

In contrast, there is substantial evidence that DGCs in chronic epileptic animals are more inhibited than those of control animals. Anatomical studies demonstrating interneuron loss also established that the remaining interneurons sprout axons, which innervate the principal neurons. This observation led to the speculation that the sprouting may compensate for the loss of inhibitory neurons (Mathern et al., 1995; Houser and Esclapez, 1996). Sprouting of mossy fiber terminals onto surviving inhibitory interneurons is an additional possible mechanism of increased inhibition observed in chronically epileptic animals (Sloviter, 1992; Sloviter et al., 2006). Electrophysiological studies have also suggested increased inhibition in animal models of TLE. Early studies demonstrated increased paired pulse inhibition in kindled animals (Tuff et al., 1983). In the kindling model, recordings of synaptic currents demonstrated an increase in the amplitude of miniature inhibitory postsynaptic currents (mIPSCs) and other studies demonstrated that the number of $GABA_A$ receptors at individual synapses was increased (Otis et al., 1994; Nusser et al., 1998). In TLE models characterized by recurrent spontaneous seizures, whole-cell $GABA_A$-receptor currents and mIPSCs recorded from DGCs were enhanced (Gibbs et al., 1997; Mtchedlishvili et al., 2001; Leroy et al., 2004).

In order to investigate whether neuropeptide-containing hilar interneurons degenerate following status epilepticus (SE) and whether this loss correlates with a persistent decrease in synaptic inhibition, we compared the number of inhibitory interneurons in the hilus of chronic epileptic animals and of animals 1, 3, and 7 days following convulsive SE with that of control animals. In parallel, GABA-mediated IPSCs were recorded from DGCs of epileptic animals and from animals that had undergone convulsive SE 1, 3, and 7 days prior to the study.

MATERIALS AND METHODS

Animal model

Experiments were performed on adult male Sprague-Dawley rats weighing 250 –300 g. The animals were injected with ketamine (50 mg/kg) and xylazine (10 mg/kg), a bipolar electrode was implanted in the left ventral hippocampus of adult rats for electrical stimulation, and EEG recordings were obtained as described previously (Lothman et al., 1990). Stereotaxic coordinates were (according to Paxinos and Watson) (in mm): AP 5.3 posterior to bregma; L 4.9; DV 5.0 below dura; incisor bar at −3.3. One week after recovery from surgery, SE was induced by the continuous hippocampal stimulation method (Lothman et al., 1989). The stimulation was set at 50 Hz, 400 μA using 1 ms biphasic square waves in 10-second trains applied every 11 seconds for 90 minutes. Self-sustaining limbic SE developed during stimulation. Approximately 4 – 6 weeks after stimulation, animals developed spontaneous limbic seizures, which were documented either by continuous EEG monitoring or direct observation of a behavioral seizure (Bertram et al., 1997).

Only animals that had prolonged electrographic SE associated with periodic epileptiform discharges on EEG were studied 1, 3, and 7 days post-SE because this pattern is predictive of later epilepsy. Animals were sacrificed 1 day (six SE-treated/six age-matched control), 3 days

(six SE-treated/six control), and 7 days (six SE-treated/six control) after SE. Although the animals in this study were not monitored by video-EEG to determine whether they had developed spontaneous seizures during the first 7 days following SE, previous studies using this model have consistently demonstrated that the shortest latency to the onset of spontaneous seizures after SE is 10 days (Bertram and Cornett, 1993; Mangan and Bertram, 1998). Because these studies used 24-hour video-EEG monitoring coupled with visual inspection of all recordings, it is unlikely that spontaneous seizures were missed.

For the study of animals with TLE, eight animals with recurrent spontaneous seizures and eight age-matched controls were used. Animals were housed at 22°C, two per cage, on a standard light/dark schedule with free access to food and water, and handled according to AALAC Animal Care and Use Guidelines and a protocol approved by the University of Virginia Animal Care and Use Committee.

Tissue preparation for immunohistochemistry

The procedures of tissue preparation were described in detail previously (Sun et al., 2004). Briefly, animals were anesthetized with an overdose of pentobarbitone sodium and perfused through the ascending aorta with 50–100 mL 0.9% NaCl followed by 350–450 mL 4% paraformaldehyde in 0.1 M phosphate buffer (PB, pH 7.4). SE-treated and epileptic animals were perfused and processed in parallel with age-matched controls. Brains were removed and postfixed in the same fixative for 2 hours at 4°C. After overnight incubation in 25% sucrose in 0.1 M PB for cryoprotection, the brains were separated into two hemispheres and the right hemisphere was blocked at 2 mm posterior to the optic tract on a coronal matrix. The left hemisphere was not studied because electrodes were implanted into the left hippocampus. Brains were frozen by immersion in −70°C isopentane. Coronal sections from the anterior block were cut at 40 μm to collect dorsal sections for other studies; the posterior block was sectioned horizontally at 40 μm. Sections of the posterior block were collected from 1 mm above the posterior commissure (horizontal section, bregma −4.1 mm) to just beneath the anterior commissure (bregma −6.82 mm). In our preliminary studies, we found that the cell loss was less consistent in dorsal hippocampus and only ventral sections were used in this study. Sections were put into 8 vials sequentially, and 6–8 ventral sections from each animal were used for each neuropeptide staining or Fluoro-Jade B experiment.

Immunohistochemistry for neuropeptide-containing interneurons

Sections were processed for free-floating immunohistochemistry, as described in detail previously (Sun et al., 2004). Following three washes in 0.1 M PB, sections were incubated with blocking solution containing 5% normal goat serum (NGS), 2% bovine serum albumin (BSA; Jackson Immunoresearch Laboratories, West Grove, PA), and 0.1% Triton X-100 in 0.1 M phosphate-buffered saline (PBS, pH 7.4) for 1 hour. Tissue sections were placed on a shaker and incubated with the primary antibodies at 4°C for 72 hours, followed by incubation in goat antirabbit or goat antimouse secondary antibodies conjugated with Alexa Fluor 488 or 594 (Molecular Probes, Eugene, OR; 5 μg/mL) for 1 hour at room temperature in darkness. All antibodies were diluted with a solution containing 1% NGS and 0.2% BSA in 0.1 M PBS. Sections were rinsed six times for 10 minutes each after incubation with the primary and secondary antibodies. Sections were mounted on slides with Gel/Mount (Biomedia, Foster City, CA) and air-dried. Each coverslip was sealed with clear nail polish, and slides were stored at −20°C. All chemicals were obtained from Sigma Chemical Co. (St. Louis, MO) except where noted.

Antibody characterization

The rabbit anti-somatostatin-28 IgG (T-4546(RGG-8004); lot No. 033988; Peninsula Laboratories, San Carlos, CA) was used in a 1:2,500 dilution. The antibody raised in rabbit

with the peptide SANSNPAMAPRERKAGCKNFF-WKTFTSC (disfulfide bond) has 100% cross-reactivity with somatostatin-28 and 25, less than 0.01% cross-reactivity with somatostatin-28 (1–12), and no cross-reactivity with somatostatin-14, prosomatostatin-32, Substance P, amylin amide (human), CCK 26-33 (nonsulfated), VIP (human, rat, porcine), and insulin (human). Preabsorption with 10 nM somatostatin-28 resulted in complete loss of immunoreactivity (Naus et al., 1988). The antigen distribution was similar to the distribution of mRNA detected by in situ hybridization (Naus and Bloom, 1988; Naus et al., 1988; Priestley et al., 1991).

A rabbit anti-cholecystokinin (CCK) Octapeptide (desulfated) IgG (T-4253(RGG7181); lot No. 032764; Peninsula Laboratories) antibody that recognizes amino acids 26–33 (DYMGWMDF, desulfated) of CCK was used in a 1:500 dilution. The antibody has 100% cross-reactivity with CCK 26-33 (desulfated), CCK 33 (porcine), caerulein, Gastrin I (human), and Big Gastrin I (human); it has some cross-reactivity with CCK 26-33 (sulfated, 78%), CCK 27-33 (62.9%), and CCK 30-33 (13.9%); however, it has no cross-reactivity with pancreatic polypeptide (human) or VIP (human, porcine, rat). The antibody has been characterized by radioimmunoassay using ^{125}I-labeled desulfated CCK octapeptide as the tracer (Innis et al., 1979). The distribution of neurons stained for CCK mRNA paralleled that of CCK-like immunoreactive neurons (Ingram et al., 1989).

A rabbit anti-neuropeptide Y (human, rat) IgG (T-4069 (RGG-7180); lot No. 017096N; Peninsula Laboratories) was used at a dilution of 1:1,000. The antibody was raised from rabbit with the antigen YPSKPDNPGEDAPAED-MARYYSALRHYINLITRQRY. The cross-reactivities with NPY (human, rat), NPY (porcine), and NPY (13-36, 16-36, 18-36, 20-36, porcine) were 100%, and the cross-reactivity with pancreatic polypeptide (human) and NPY 22-36 (porcine) was 1.6% and 1.5%, respectively. However, there was no cross-reactivity with NPY 26-36, Peptide YY, VIP (human, porcine, rat), amylin (human), insulin (human), and somatostatin. Incubation of tissue sections with antiserum preabsorbed with 10 nmol of synthetic NPY in a liquid absorption test completely blocked the immunostaining (Chan-Palay et al., 1986). The distribution of the antigen immunoreactivity was similar to that of the mRNA in situ hybridization (Vezzani et al., 1996).

A mouse antiparvalbumin (PV) (Clone PARV-19; P 3088; lot No. 064K4777; Sigma) was diluted at 1:2,000. This antibody (mouse IgG1 isotype) is derived from the PARV-19 hybridoma produced by the fusion of mouse myeloma cells and splenocytes from an immunized mouse. This antiserum was raised against purified frog muscle PV and reacts specifically with PV (12 kDa) originating from human, bovine, goat, pig, rabbit, dog, cat, rat, frog, and fish. The antibody does not react with other members of the EF-hand family such as calmodulin, intestinal calcium-binding protein, S100A2, S100A6 (calcyclin), the α-chain of S-100, or the β-chain, myosin light chain, and troponin. Incubation of tissue sections with the antibody preabsorbed with purified rat muscle PV in a liquid absorption test completely blocked the immunostaining (Celio, 1990). The distribution of PV revealed by in situ hybridization was in agreement with immunoreactivity revealed by this antibody (Seto-Ohshima et al., 1989). Controls in which the primary antibody was omitted resulted in no staining.

Fluoro-Jade B labeling

In order to assess neurodegeneration, Fluoro-Jade B (Chemicon, Temecula, CA) staining was performed. Briefly, tissue sections were mounted on slides and air-dried on a slide warmer at 50°C for at least 30 minutes. The slides were immersed in a solution containing 1% sodium hydroxide in 80% alcohol for 5 minutes, and in 70% alcohol followed by distilled water for 2 minutes each. The slides were transferred to a solution of 0.06% potassium permanganate for 10 minutes on a shaker to ensure consistent suppression of background staining, and rinsed in

distilled water for 2 minutes. The staining solution was 0.0003% Fluoro-Jade B in 0.1% acetic acid prepared within 10 minutes of use from a 0.01% Fluoro-Jade B stock solution. After 20 minutes in the staining solution, the slides were rinsed for 1 minute in each of three distilled water washes. The slides were placed on a slide warmer until they were fully dry. The dry slides were cleared by immersion in xylene for at least 1 minute before placing the coverslip with DPX mounting medium.

In order to stain for neuropeptides and Fluoro-Jade B, the Fluoro-Jade B immunohistochemical technique was modified (Jakab and Bowyer, 2002). Sections were incubated for 48 hours at 4°C in the antineuropeptide primary antibody followed by incubation with a secondary antibody conjugated to Alexa Fluor 594 (5 μg/mL; Molecular Probes) for 60 minutes at room temperature. Sections were wet-mounted on glass slides, air-dried at 50°C for 15 minutes, and stained with Fluoro-Jade B. The slides were immersed in distilled water for 1 minute and oxidized in a 0.006% solution of $KMnO_4$ for 5 minutes. After rinsing in distilled water twice for 30 seconds, sections were stained for 10 minutes in a 0.0003% solution of Fluoro-Jade B in 0.1% acetic acid. Finally, sections were rinsed in distilled water, air-dried, and cleared with xylene.

Image acquisition and analysis

Sections were studied on a Nikon PCM2000 confocal microscope system as described in detail previously (Sun et al., 2004). All confocal laser scanning microscopy was performed at the W.M. Keck Center for Cellular Imaging at the University of Virginia. A Nikon (Melville, NY) TE-200 inverted epifluorescence microscope was equipped with an argon and a HeNe laser. Confocal and camera-based image acquisition and processing were driven by SimplePCI software (v. 4.0.6, Compix, Cranberry Township, PA). Argon-ion and HeNe lasers were used to visualize the fluorochromes, Fluoro-Jade B and Alexa Fluor 594, respectively. The intensity of each laser was optimized for the sections of each animal and each combination of antibodies. The parameters were kept constant for each animal. Controls included dual-channel recording of sections without antigen labeling and single antigen labeling to detect nonspecific staining and bleed-through phenomena.

The dentate gyrus was scanned and captured with a low-magnification objective lens (10×). For double labeling of Fluoro-Jade B and neuropeptide experiments, separate scanning was performed for different channels to avoid high bleed-through. For quantitative analysis of profiles in the hilus of the dentate gyrus, a contour of the hilus was drawn along the outer border of the DGC layer and straight lines were drawn from the ends of the granule cell layer to the proximal end of the CA3 pyramidal cell layer (Kobayashi and Buckmaster, 2003). Profiles within the contour were quantified using MetaMorph 6.03 software (Universal Imaging, Downingtown, PA). The same threshold was applied to all images acquired from the sections of one brain in each experiment. Most of these antigens were revealed as individual profiles, which were considered individual objects in binary images. An aggregation of 50 – 800 pixels (72–1,152 μm^2) of intensity at least twice the background intensity was considered a profile that represents a cell soma. Data were analyzed using Prism 4.0 software (GraphPad Software, San Diego, CA). Unless specified otherwise, all values are reported as mean ± SEM.

Somatostatin silver enhancement staining for electron microscope

Three animals that had undergone SE 3–7 days prior to study and two age-matched controls were used to investigate the SOM-IR soma and profiles in the dentate hilus and the outer molecular layer of the hippocampus. Animals were perfused transcardially with Tyrode solution (a balanced salt solution composed of 137 mM NaCl, 2 mM KCl, 0.9 mM $CaCl_2$, 1.2 mM $MgCl_2$, 11.9 mM $NaHCO_3$, 0.4 mM NaH_2PO_4, 5.5 mM glucose, pH 7.4, osmotic strength 281 mOsm). This solution improves the ultrastructure of tissue (Heck et al., 2002). A fixative

consisting of 4% paraformaldehyde and 0.1% glutaraldehyde in 0.1 M PB was perfused until the effluent was clear. Brains were removed from the skulls and postfixed in 4% paraformaldehyde for 2 hours at 4°C, and cut in PB by a vibratome at a thickness of 50 μm. Sections were treated with 0.1% $NaBH_4$ at room temperature for 30 minutes and rinsed with PB. Sections were incubated in 0.05% Triton X-100 in PB for 30 minutes at room temperature, rinsed four times for 10 minutes each, and blocked in a solution consisting of 5% BSA, 0.2% cold-water fish skin gelatin (CWFS gelatin), and 5% NGS for 30 minutes at room temperature. Sections were rinsed twice for 10 minutes with a solution consisting of 0.2% Auron acetylated bovine serum albumin (BSA-c), and incubated with rabbit anti-SOM antibody (1:500, diluted with a solution containing 1% BSA, 0.05% NaN_3 in 0.1 M PBS) for 70 hours at room temperature. Sections were rinsed with PBS/BSA-c six times for 10 minutes, incubated with goat antirabbit IgG conjugated with biotin (1:200), and rinsed with fresh PBS/BSA-c six times for 10 minutes. Sections were incubated with streptavidin conjugated with ultrasmall gold (1:100, diluted in PBS/BSA-c) for 16 hours at 4°C, rinsed with PBS/BSA-c six times for 10 minutes each, and rinsed with PB twice for 10 minutes each. Sections were washed with Enhancement Conditioning Solution (ECS), four times for 10 minutes each. Silver enhancement was done with R-Gent SE-EM electron microscopy grade silver enhancement mixture (Aurion, Wageningen, Netherlands) for 90 minutes. Enhancement was terminated with 0.03 M sodium thiosulfate in ECS for 10 minutes, rinsed with ECS four times for 10 minutes each, and with PB twice for 10 minutes each. Sections were put in 0.5% osmium tetroxide in PB for 15 minutes, dehydrated, and flat-embedded in Epon 812 resin (Electron Microscopy Sciences, Fort Washington, PA) between two sheets of Aclar film (Electron Microscopy Sciences). After resin polymerization, small sections including the molecular layer, granule cell layer, and part of the hilus were dissected from the ventral hippocampus and mounted on capsules. Ultrathin sections at the interface of tissue and resin were collected and stained with uranyl acetate and lead citrate. Grids were examined on a Jeol JEM 1010 microscope, and images were captured by a 16 megapixel SIA-12C (sia-cam.com) digital camera coupled with MaxIm DL CCD software (Diffraction Limited, Ottawa, Canada).

Voltage-clamp recordings

For electrophysiological experiments, another group of eight epileptic animals and eight age-matched controls were studied. In addition, five animals of each were studied 1, 3, and 7 days after SE along with age-matched controls. Animals were anesthetized with halothane prior to decapitation. Brains were immersed in ice-cold (2–4°C) artificial cerebro-spinal fluid (ACSF) saturated with 95%O_2/5%CO_2. The ACSF consisted of (in mM): NaCl 127, KCl 2, $CaCl_2$1.5, $MgSO_4$ 1.5, $NaHCO_3$ 25.7, KH_2PO_4 1.1, glucose 10 (300–305 mOsm). Brains were divided into two hemispheres longitudinally. The right hemisphere, which was contralateral to the stimulated side, was mounted on a vibratome stage (Camden Instruments, UK) and coronal sections (300 μm) containing ventral part of the dentate gyrus were obtained. Slices were maintained in continuously oxygenated ASCF at 32°C for at least 30–45 minutes before transfer to the recording chamber, which was mounted on the stage of an Olympus BX51 microscope equipped with DIC-IR optics with video monitoring and a 40× water-immersion objective. In the recording chamber, slices were continuously super-fused with ACSF saturated with 95%O_2/5%CO_2 at room temperature (22–24°C). Patch electrodes were pulled from borosilicate glass (Sutter Instruments, Novato, CA) on a horizontal Flaming-Brown microelectrode puller (model P-97, Sutter Instruments) using a 2-stage pull protocol. Electrode resistances were 4–6 M°. Electrode tips were filled with an internal recording solution consisting of (in mM): CsCl 153.3, $MgCl_2$ 1.0, N-[2-Hydroxyethyl]piperazine-N-[2-ethansulfonic acid] (HEPES) 10.0, and glycol-bis(α-aminoethyl ether) N,N,N,N-tetraacetic acid (EGTA) 5.0, pH 7.2 (with CsOH); 285–295 mOsm; the internal solution was sterile-filtered before use. The electrode shank contained an addition of 3.5 mM ATP. Visually identified DGCs were voltage-clamped to −65 mV with an Axopatch 200B amplifier (Axon

Instruments, Union City, CA). Whole cell capacitance and series resistance were compensated by 75–80% at 10 μs lag. A recording was performed when series resistance after compensation was 20 M° or less. Access resistance was monitored with a 10 ms, −5 mV test pulse once every 2 minutes. The recording was rejected when the series resistance increased by 25% during the experiment. Data were acquired on a computer hard drive at 5 kHz using a Digidata 1322 digitizer and Axoscope 8.0 software (Axon Instruments). Current traces were analyzed with Mini Analysis software (Synaptosoft, Leonia, NJ).

The digital images selected for publication were processed in PhotoShop 6.0 (Adobe, San Jose, CA). For each antibody a contrast/brightness setting was selected that yielded a high-resolution image for both bright and dim sections without exceeding a maximal pixel intensity of 255.

RESULTS

Loss of somatostatin-containing hilar interneurons

Images of ventral hippocampal sections including the hilus were obtained using a confocal laser scanning microscope with a 10× (NA: 0.3) lens to examine SOM-IR neurons in control and epileptic animals. The morphology and distribution of SOM-IR neurons in the hilus of the dentate gyrus obtained from control animals were similar to that described in detail previously (Milner and Bacon, 1989; Leranth et al., 1990; Esclapez and Houser, 1995). Numerous SOM-IR cells were present in the hilus and some were found in the margin of the DGC layer. The cells were of two kinds in size: large multipolar stained cells and small cells. There was a dense SOM-IR plexus in the outer molecular layer, and some less intense diffuse fibers were found in the inner and middle molecular layers and granule cell layer. We tested whether SOM-IR neurons were diminished in chronically epileptic animals. Visual examination of the images suggested that there were fewer SOM-IR cells present in epileptic animals than in controls (Fig. 1). Compared with sections from control animals (56 ± 1.9 cells per section, n = 46 sections, 6 animals) the number of SOM-containing interneurons in the dentate hilus of epileptic animals (49 ± 2.7, n = 40 sections, 6 animals, Fig. 1E–G, Table 1) was diminished.

In order to determine when somatostatin-containing interneurons begin to degenerate, we assessed the time course of the reduction of SOM-IR interneurons (Fig. 1A–D). The SOM-IR profiles in the hilus were counted in each section obtained from ventral hippocampus of control and SE-treated animals 1, 3, and 7 days following treatment. The number of SOM-IR cells in the hilus was diminished at each timepoint following SE (Fig. 1F,G, Table 1).

Because the reduction of SOM-IR interneurons can result from neurodegeneration, Fluoro-Jade B staining of hippocampal sections was performed to evaluate potential neurodegeneration. Neuronal damage peaks at 24 hours following SE but continues up to an additional 48 hours (Fujikawa, 1996); therefore, we examined SOM-IR and Fluoro-Jade B staining in serial sections 72 hours after the onset of SE. Whereas no cells were stained with Fluoro-Jade B in sections from control animals, SE-treated animals demonstrated stained cells throughout the hilus. Hippocampal sections that had a large number of Fluoro-Jade B-staining cells were from animals that demonstrated extensive loss of SOM-IR neurons; few Fluoro-Jade B-staining cells were present in sections from animals that showed limited loss of SOM-IR. There was a correlation between neuronal loss and loss of SOM-IR cells in serial sections (Pearson's correlation, $r = -0.82$, $P < 0.001$, n = 24 pairs of sections from five animals), consistent with previous studies in the kainate model of TLE (Buckmaster and Dudek, 1997; Kobayashi and Buckmaster, 2003). Therefore, we tested whether some of the Fluoro-Jade B-stained cells were also SOM-IR. Sections from SE-treated animals were double-stained for SOM and Fluoro-Jade B, separate scans were obtained for each fluorophore, and these images were combined to assess double staining. There were several examples of cells that stained for Fluoro-Jade B and SOM (Fig. 2A–C, arrowheads). A quantitative evaluation of colocalization

of Fluoro-Jade B and SOM revealed 1.8 ± 0.3 (n = 29 sections, five SE-treated animals) cells per section that were immunoreactive for both SOM and Fluoro-Jade B.

Electron microscopic studies to confirm neurodegeneration of SOM-containing interneurons

To corroborate the light microscopic findings that the reduction of SOM-IR neurons following SE was due possibly to degeneration of SOM-containing interneurons, an electron microscopic study was performed on sections from animals that were 3–7 days post-SE.

Preembedding silver-enhanced staining of SOM was performed on sections from the hippocampi of control animals and 3–7 days post-SE. Control animal hippocampi demonstrated SOM immunostaining of the neuronal perikarya, dendrites, axons, and terminals (Fig. 3A,C), similar to that described in previous studies (Milner and Bacon, 1989; Leranth et al., 1990). In the hilus of the hippocampi from SE-treated animals there were some degenerating SOM-IR interneurons, as demonstrated by perinuclear vacuoles and chromatin condensation (Fig. 3B,D). In sections from control animals there were dendrites and terminals of SOM interneurons in the outer molecular layer (Fig. 4A,C). In sections from 3–7 days post-SE animals, vacuoles and mitochondrial condensation were found in degenerating SOM-IR dendrites (Fig. 4B,D). These EM data corroborated the finding that some SOM-IR interneurons were degenerating at 3–7 days post-SE.

Neuropeptide Y-containing interneurons

Many SOM-containing interneurons also express neuropeptide Y (NPY) (Kohler et al., 1987; Deller and Leranth, 1990); therefore, we expected a reduction in the number of NPY-containing interneurons. Indeed, we found the number of NPY-IR cells in the hilus of epileptic animals was decreased compared to controls. This reduction in NPY-IR interneurons was apparent 3 and 7 days following SE but not 1 day following SE (Fig. 5A–G, Table 1). Degeneration of NPY-IR cells was confirmed by staining hippocampal sections for Fluoro-Jade B and NPY. As illustrated (arrowheads in Fig. 2D–F), neurons double-labeled for Fluoro-Jade B and NPY were present in the hilus of animals 1 day following SE. Detailed quantification of 21 sections from three animals studied 1 day following SE demonstrated a colocalization of NPY and Fluoro-Jade B of 2 ± 0.5 cells per section.

Basket cells after status epilepticus

Basket cells are a group of interneurons that mediate inhibition of granule cell soma and proximal dendrites. Two neurochemically distinct classes of cells constitute basket cells, the PV-immunoreactive (IR) interneurons and CCK-IR interneurons. PV-IR neurons are located at the margin of the granule cell layer and the hilus, and others are distributed in the hilus and CA3c area (Fig. 6A). In addition, dense PV-IR fibers outline granule cells in the granule cell layer and some processes throughout the molecular layer. The number of PV-containing interneurons in the dentate hilus in hippocampal sections from chronic epileptic animals (10 ± 0.8, n = 46 sections, six animals) and in sections from control animals (9 ± 0.8, n = 61 sections, six animals) was similar (Fig. 6A,E–G, Table 1).

In contrast, the number of PV-IR interneurons was diminished 1, 3, and 7 days following SE (Fig. 6B–D, Table 1); however, there was no evidence of degeneration of these neurons at these timepoints. Hippocampal sections from animals 1 day after SE were stained for Fluoro-Jade B and PV to determine whether degeneration of PV-containing interneurons had occurred. As illustrated in Figure 2, there were no neurons double-labeled for Fluoro-Jade B and PV in the hilus of these animals (Fig. 2G–I). To corroborate this finding, sections from animals 3 days following SE were also double-labeled for Fluoro-Jade B and PV, and no double-labeled cells were found (15 sections from three animals). These experiments suggested the possibility that

reduction in the number of PV-staining interneurons was a transient reduction in neuropeptide expression and did not represent neurodegeneration of these neurons (Fig. 6E–G).

CCK-IR interneurons were assessed to determine their potential loss following SE. Consistent with previous studies (Freund and Buzsaki, 1996), CCK-IR neurons were found in the hilus of the dentate gyrus, most of these cells were located at the margin between the granule cell layer and the hilus (Fig. 7A), and CCK-IR fibers were found in the inner and middle molecular layer as well. The number of CCK-IR neurons in the hilus of epileptic animals was similar to that in controls (Fig. 7E–G, Table 1). The number of CCK-IR neurons was unchanged 1 day after SE (Fig. 7B,F,G, Table 1), but was diminished 3 and 7 days after SE (Fig. 7C,D,F,G, Table 1). We investigated whether CCK-IR neurons had undergone neurodegeneration by testing for colocalization of Fluoro-Jade B staining and CCK-IR. In 18 sections from three animals, none of the Fluoro-Jade B-stained cells colocalized with CCK-IR cells (Fig. 2J–L).

IPSC frequency

Neuroanatomical studies suggested that SE resulted in the degeneration of GABAergic interneurons containing SOM and/or neuropeptide Y. These interneurons are known to make GABA-containing symmetric synapses on the dendrites of granule cells. Therefore, we investigated the frequency of inhibitory synaptic currents following SE. Spontaneous IPSCs (sIPSCs) were recorded from DGCs using whole-cell patch-clamp electrophysiology after blocking excitatory transmission with AP-5 and CNQX. Addition of 10 μM bicuculline methiodide abolished IP-SCs, demonstrating that they were mediated by $GABA_A$ receptors (data not shown). Recordings were started 5 minutes after rupturing the seal to ensure complete dialysis of the cell contents with intracellular solution.

The frequency of sIPSCs recorded from DGCs of epileptic animals was 52% of that recorded from controls. The sIPSC frequency was also reduced in the period following convulsive SE reaching a nadir at 7 days (Fig. 8). The frequency of sIPSCs recorded from DGCs of epileptic animals tended to be more than that recorded from animals 7 days following SE (Fig. 8); however, it was significantly less than that recorded from age-matched controls (Fig. 8A). Loss of interneurons should diminish both action potential-dependent and -independent neurotransmitter release. To address this issue, we blocked all action potentials and recorded miniature IPSCs (mIPSCs). The frequency of mIPSCs recorded from DGCs of epileptic animals was only 35% of that recorded from controls. Similarly, the frequency of mIPSCs recorded from DGCs 7 days following SE was 30% of that recorded from control DGCs (Fig. 8E).

The reduction in the frequency of sIPSCs recorded from DGCs of animals that had undergone SE appeared to follow the time course of the reduction in the number of SOM-IR neurons in the hilus following SE. A quantitative evaluation revealed a strong correlation between the numbers of SOM-containing interneurons and sIPSC frequency at various timepoints ($r = 0.9$, $P < 0.05$, Fig. 8F). This suggested that the reduction of SOM-IR might have caused reduction in sIPSC frequency. Previous studies and the present light and electron microscopic studies demonstrate that SOM-containing interneurons preferentially make synapses on distal dendrites of DGCs. Synaptic currents generated at distal dendrites are remote from the patch-recording pipette and are filtered due to cable properties of dendrites. Because dendritic filtering can cause an attenuation of IPSC rise times, we tested whether slow rise time events were selectively removed from the population of events.

A frequency distribution histogram of 10 –90% rise times of ~7,500 mIPSCs recorded from six control DGCs was constructed. Rise times were binned to 0.1-ms bin sizes and fit to multiple Gaussian distributions. The data were fit best to three distinct populations representing rapid, intermediate, and slow rise time events. In recordings from control DGCs, 28% of the events

were rapid, 37% were intermediate rise time, and 34% were slow rise time events (Fig. 9A). When ~1,300 mIPSCs recorded from DGCs of animals 7 days post-SE were analyzed, a dramatically different distribution emerged. Slow events were rare and represented only 1% of all events (Fig. 9B). Among mIPSCs recorded from epileptic animals, there were a larger number of slow events, but their proportion was still less than that obtained from controls. In epileptic animals, slow rise time events made up 18% of the total number of events, whereas slow rise time events in controls were 34% (Fig. 9C). This selective loss of slow rise time events was suggestive of loss of distal synapses and was consistent with loss of SOM interneurons.

DISCUSSION

This study demonstrated loss and degeneration of SOM-and NPY-IR neurons in the hilus of the dentate gyrus of animals that had undergone SE and developed TLE. Several independent experiments supported these conclusions: 1) the number of SOM- and NPY-IR neurons decreased following SE and remained diminished in chronically epileptic animals; 2) there was an inverse correlation between the number of Fluoro-Jade B-stained cells and SOM-IR neurons, and there were examples of Fluoro-Jade B stained-cells with SOM- or NPY-immunostaining in the dentate hilus; 3) electron microscopic analysis of SOM-IR neurons revealed degenerating cell bodies and synaptic profiles; and 4) the loss of SOM-IR neurons correlated with a reduction in IPSC frequency, and there was preferential loss of slow rise-time IPSCs consistent with a loss of distal synapses of SOM-IR neurons. These anatomical and electrophysiological data together demonstrate degeneration of hilar interneurons resulting in a diminished inhibitory synaptic transmission onto distal dendrites of DGCs in an animal model of chronic TLE.

In epileptic foci induced by alumina gel applied to the neocortex of monkeys, there was loss of GABAergic nerve terminals and symmetric synapses (Ribak et al., 1979, 1982). Previous studies using animal models of TLE have demonstrated a reduced number of SOM-containing inter-neurons in the dentate hilus and the CA1 pyramidal region (Sloviter and Nilaver, 1987; Schwarzer et al., 1995; Buckmaster and Dudek, 1997; Cossart et al., 2001; Kobayashi and Buckmaster, 2003). In hippocampi surgically removed from patients with mesial temporal sclerosis, there is evidence of a reduced number of SOM-IR interneurons (de Lanerolle et al., 1989; Robbins et al., 1991; Mathern et al., 1995). Initial studies suggested that SOM-IR interneurons did not contain GABA (Sloviter and Nilaver, 1987). However, later electron microscopic studies convincingly demonstrated that SOM-IR interneurons made symmetric synapses on granule cells (Leranth et al., 1990). Other studies demonstrated that interneurons that expressed SOM mRNA also expressed mRNA for the GABA synthetic enzyme GAD 65 (Esclapez and Houser, 1995). Furthermore, somal GABA was convincingly demonstrated in all hippocampal interneurons (Sloviter et al., 2001).

One limitation of immunohistochemical studies demonstrating a diminished number of SOM-IR interneurons in the hilus is the possibility that these interneurons simply stopped producing SOM without degenerating and therefore would not be detected on immunohistochemistry. In the absence of direct evidence of degeneration of these neurons, previous studies relied on the correlation of hilar cell counts in Nissl-stained sections and those sections stained for SOM (Buckmaster and Dudek, 1997; Kobayashi and Buckmaster, 2003). The present study demonstrates the degeneration of SOM-IR cells following SE for the first time by the colocalization of Fluoro-Jade B with SOM-IR interneurons; Fluoro-Jade B is a high-affinity fluorescent marker commonly used to identify degenerating neurons, and is more specific and has less background staining compared with the original Fluoro-Jade (Schmued and Hopkins, 2000).

The present study also provided electron microscopic evidence of degeneration of SOM-IR neurons and dendritic profiles following SE. In TLE models, electron microscopic evidence of granule cell loss has been presented in the past (Sloviter et al., 1996), but similar evidence for degeneration of SOM interneuron in the hilus has not been reported. Degenerating SOM terminals were not found in the outer molecular layer, perhaps because the transport of SOM to the terminals may be arrested in the early stages of neurodegeneration. Alternatively, SOM that is present in the terminals may be lost during SE. The degeneration of interneurons may have been more obvious if the neurons were studied after a longer interval following SE; however, SOM immunoreactivity would be lost at that time. Therefore, we studied SOM interneurons 3–7 days following SE to increase the likelihood of detecting SOM antigen in the dying cell.

NPY cell reduction

The number of NPY-IR profiles in the hilus of the dentate gyrus was decreased compared with controls, whereas some of the NPY-IR cells of the granule cell layer survived. A similar loss of NPY-containing interneurons in the hilus was reported previously (Sloviter et al., 2003). Following SE, several hilar neurons stained for NPY and Fluoro-Jade B. Furthermore, there was a significant correlation between the number of NPY-IR cells and the number of Fluoro-Jade B-labeled cells in the hilus. This suggested that the NPY-IR cell loss was due to cell death. Many hilar interneurons that express NPY also express SOM, and it is possible that this subset of interneurons is selectively vulnerable to injury following SE. Mossy fibers in the hilus stained for NPY, and a dense band of NPY staining was found in the inner molecular layer of TLE animals, consistent with mossy fiber sprouting in epileptic animals (Schwarzer et al., 1995).

There was transient reduction of PV-IR interneurons 3–7 days after SE, but the number of PV-IR interneurons in epileptic animals was similar to that in controls. Fluoro-Jade B colocalization studies found no evidence of neurodegeneration of PV-IR interneurons. These observations suggest that following SE there was transient down-regulation of PV production that recovered over several weeks. Similar findings were reported in the perforant path model of TLE, where it was suggested that reduced immunoreactivity and mRNA of PV was due to reduced expression instead of cell death (Sloviter et al., 2003). However, PV-IR was found reduced in the pilocarpine model of TLE (Kobayashi and Buckmaster, 2003) and may reflect differences in the animal models. Another possibility is that only a small number of PV cells was lost and our cell counting methods missed this cell loss.

Physiological consequences of loss of SOM/NPY interneurons

The current study found that the frequency of sIPSCs and mIPSCs was reduced following SE and it remained diminished in chronically epileptic animals. One likely explanation for these results is the loss of SOM-IR neurons and terminals. The reduction of sIPSC frequency followed a time course similar to the loss of SOM-IR neurons. According to Katz's model of synaptic transmission, a reduction of the frequency of synaptic events can result from a diminished frequency of action potentials in the presynaptic terminals, a diminished probability of release from GABAergic terminals in response to an action potential, a diminished number of terminals, or a combination of these factors. However, mIPSCs occur independent of action potentials, thereby eliminating the potential contribution of action potentials and action potential-mediated synaptic release. Therefore, a reduction of mIPSC frequency supports the loss of GABAergic terminals. In addition, selective loss of slow rise time mIPSCs supported the hypothesis that loss of GABAergic terminals resulted in a reduced frequency of IPSCs. Some previous studies have suggested that loss of SOM-IR neurons does not contribute to inhibition of DGCs (Sloviter, 1987). More recent studies have reported diminished frequency of IPSCs in DGCs of animals made epileptic with kainate or pilocarpine (Kobayashi and

Buckmaster, 2003; Shao and Dudek, 2005). A similar reduction of SOM-IR neurons was associated with a reduced frequency of IPSCs in CA1 pyramidal neurons in pilocarpine-induced epilepsy (Cossart et al., 2001).

The physiological consequences of the loss of distal synaptic inhibition described in this study are uncertain. It is possible that reduced GABAergic synaptic input from somatostatin-containing interneurons to DGCs contributes to their hyperexcitability. However, one study has suggested that mIPSCs generated in distal dendrites do not contribute to the inhibition of the DGC soma (Soltesz et al., 1995). Additionally, a small (13%) reduction in the number of interneurons was observed in this study and this reduction may not fully explain the observed reduction in IPSC frequency; additional changes in release machinery may have a contribution. Furthermore, these physiological findings may not extend to all animal models of TLE. For example, in the perforant path model of TLE, there is almost complete loss of hilar interneurons and it is likely that such profound neuronal loss would have different physiological consequences.

Only a small fraction of Fluoro-Jade B-positive cells colocalized with interneurons markers, suggesting that a majority of dying neurons were mossy cells. Previous studies have suggested that loss of mossy cells results in the loss of excitatory inputs into PV- and CCK-containing basket cells, leading to diminished inhibition of DGCs in epileptic animals (Sloviter, 1991; Bekenstein and Lothman, 1993). Dormancy of basket cells was not directly tested in this study because both sIPSCs and mIPSCs were recorded from DGCs in the absence of all excitatory transmission. Any reduction in excitatory drive onto basket cells could further add to the reduced frequency of IPSCs described in this study. Other changes in the structure and connectivity of DGCs could contribute to their hyperexcitability, including loss of mossy cells and dormancy of basket cells (see above), changes in the expression of $GABA_A$ receptors (Coulter, 2001), NMDA receptors (Mody and Heinemann, 1987), calcium channels (Mody, 1998), and potassium channels (Bender et al., 2003), and mossy fiber sprouting (Tauck and Nadler, 1985; Wuarin and Dudek, 1996).

Acknowledgments

We thank Drs. Kevin Kelly and Howard Goodkin for editing the article.

Grant sponsor: National Institute of Neurological Disorders and Stroke (NINDS); Grant numbers: RO1 NS40337, RO1NS044370, RO1 NS025605.

Abbreviations

CCK	Cholecystokinin
DGC	Dentate granule cell
IR	Immunoreactive
NPY	Neuropeptide Y
PV	Parvalbumin
SE	Status epilepticus
SOM	Somatostatin
TLE	Temporal lobe epilepsy

LITERATURE CITED

Bekenstein JW, Lothman EW. Dormancy of inhibitory interneurons in a model of temporal lobe epilepsy. Science 1993;259:97–100. [PubMed: 8093417]

Bender RA, Soleymani SV, Brewster AL, Nguyen ST, Beck H, Mathern GW, Baram TZ. Enhanced expression of a specific hyperpolarization-activated cyclic nucleotide-gated cation channel (HCN) in surviving dentate gyrus granule cells of human and experimental epileptic hippocampus. J Neurosci 2003;23:6826–6836. [PubMed: 12890777]

Bertram EH, Cornett J. The ontogeny of seizures in a rat model of limbic epilepsy: evidence for a kindling process in the development of chronic spontaneous seizures. Brain Res 1993;625:295–300. [PubMed: 8275310]

Bertram EH, Williamson JM, Cornett JF, Spradlin S, Chen ZF. Design and construction of a long-term continuous video-EEG monitoring unit for simultaneous recording of multiple small animals. Brain Res Brain Res Protoc 1997;2:85–97. [PubMed: 9438076]

Buckmaster PS, Dudek FE. Neuron loss, granule cell axon reorganization, and functional changes in the dentate gyrus of epileptic kainate-treated rats. J Comp Neurol 1997;385:385–404. [PubMed: 9300766]

Celio MR. Calbindin D-28k and parvalbumin in the rat nervous system. Neuroscience 1990;35:375–475. [PubMed: 2199841]

Chan-Palay V, Kohler C, Haesler U, Lang W, Yasargil G. Distribution of neurons and axons immunoreactive with antisera against neuropeptide Y in the normal human hippocampus. J Comp Neurol 1986;248:360–375. [PubMed: 3522662]

Cossart R, Dinocourt C, Hirsch JC, Merchan-Perez A, De Felipe J, Ben Ari Y, Esclapez M, Bernard C. Dendritic but not somatic GABAergic inhibition is decreased in experimental epilepsy. Nat Neurosci 2001;4:52–62. [PubMed: 11135645]

Coulter DA. Epilepsy-associated plasticity in gamma-aminobutyric acid receptor expression, function, and inhibitory synaptic properties. Int Rev Neurobiol 2001;45:237–252. [PubMed: 11130901]

Del Castillo J, Katz B. Biophysical aspects of neuromuscular transmission. Prog Biophys Biophys Chem 1956;6:121–170. [PubMed: 13420190]

de Lanerolle NC, Kim JH, Robbins RJ, Spencer DD. Hippocampal interneuron loss and plasticity in human temporal lobe epilepsy. Brain Res 1989;495:387–395. [PubMed: 2569920]

Deller T, Leranth C. Synaptic connections of neuropeptide Y (NPY) immunoreactive neurons in the hilar area of the rat hippocampus. J Comp Neurol 1990;300:433–447. [PubMed: 2266195]

Esclapez M, Houser CR. Somatostatin neurons are a subpopulation of GABA neurons in the rat dentate gyrus: evidence from colocalization of pre-prosomatostatin and glutamate decarboxylase messenger RNAs. Neuroscience 1995;64:339–355. [PubMed: 7700525]

Freund TF, Buzsaki G. Interneurons of the hippocampus. Hippocampus 1996;6:347–470. [PubMed: 8915675]

Fujikawa DG. The temporal evolution of neuronal damage from pilocarpine-induced status epilepticus. Brain Res 1996;725:11–22. [PubMed: 8828581]

Gibbs JW, Shumate MD, Coulter DA. Differential epilepsy-associated alterations in postsynaptic $GABA_A$ receptor funcction in dentate granule and CA1 neurons. J Neurophysiol 1997;77:1924–1938. [PubMed: 9114245]

Heck WL, Slusarczyk A, Basaraba AM, Schweitzer L. Subcellular localization of GABA receptors in the central nervous system using post-embedding immunohistochemistry. Brain Res Brain Res Protoc 2002;9:173–180. [PubMed: 12113777]

Houser CR, Esclapez M. Vulnerability and plasticity of the GABA system in the pilocarpine model of spontaneous recurrent seizures. Epilepsy Res 1996;26:207–218. [PubMed: 8985701]

Ingram SM, Krause RG, Baldino F Jr, Skeen LC, Lewis ME. Neuronal localization of cholecystokinin mRNA in the rat brain by using in situ hybridization histochemistry. J Comp Neurol 1989;287:260–272. [PubMed: 2794128]

Innis RB, Correa FM, Uhl GR, Schneider B, Snyder SH. Cholecystokinin octapeptide-like immunoreactivity: histochemical localization in rat brain. Proc Natl Acad Sci U S A 1979;76:521–525. [PubMed: 284371]

Jakab RL, Bowyer JF. Parvalbumin neuron circuits and microglia in three dopamine-poor cortical regions remain sensitive to amphetamine exposure in the absence of hyperthermia, seizure and stroke. Brain Res 2002;958:52–69. [PubMed: 12468030]

Kapur J, Stringer JL, Lothman EW. Evidence that repetitive seizures in the hippocampus cause a lasting reduction of GABAergic inhibition. J Neurophysiol 1989;61:417–426. [PubMed: 2918363]

Kobayashi M, Buckmaster PS. Reduced inhibition of dentate granule cells in a model of temporal lobe epilepsy. J Neurosci 2003;23:2440–2452. [PubMed: 12657704]

Kohler C, Eriksson LG, Davies S, Chan-Palay V. Co-localization of neuropeptide tyrosine and somatostatin immunoreactivity in neurons of individual subfields of the rat hippocampal region. Neurosci Lett 1987;78:1–6. [PubMed: 2886960]

Leranth C, Malcolm AJ, Frotscher M. Afferent and efferent synaptic connections of somatostatin-immunoreactive neurons in the rat fascia dentata. J Comp Neurol 1990;295:111–122. [PubMed: 1971287]

Leroy C, Poisbeau P, Keller AF, Nehlig A. Pharmacological plasticity of GABA(A) receptors at dentate gyrus synapses in a rat model of temporal lobe epilepsy. J Physiol 2004;557:473–487. [PubMed: 15034126]

Lothman EW, Bertram EH, Bekenstein JW, Perlin JB. Self-sustaining limbic status epilepticus induced by 'continuous' hippocampal stimulation: electrographic and behavioral characteristics. Epilepsy Res 1989;3:107–119. [PubMed: 2707248]

Lothman EW, Bertram EH, Kapur J, Stringer JL. Recurrent spontaneous hippocampal seizures in the rat as a chronic sequela to limbic status epilepticus. Epilepsy Res 1990;6:110–118. [PubMed: 2387285]

Mangan PS, Bertram EH III. Ontogeny of altered synaptic function in a rat model of chronic temporal lobe epilepsy. Brain Res 1998;799:183–196. [PubMed: 9675275]

Mathern GW, Babb TL, Pretorius JK, Leite JP. Reactive synaptogenesis and neuron densities for neuropeptide Y, somatostatin, and glutamate decarboxylase immunoreactivity in the epileptogenic human fascia dentata. J Neurosci 1995;15:3990–4004. [PubMed: 7751960]

McNamara JO. Emerging insights into the genesis of epilepsy. Nature 1999;399:A15–A22. [PubMed: 10392576]

Milner TA, Bacon CE. Ultrastructural localization of somatostatin-like immunoreactivity in the rat dentate gyrus. J Comp Neurol 1989;290:544–560. [PubMed: 2613944]

Mody I. Ion channels in epilepsy. Int Rev Neurobiol 1998;42:199–226. [PubMed: 9476174]

Mody I, Heinemann U. NMDA receptors of dentate gyrus granule cells participate in synaptic transmission following kindling. Nature 1987;326:701–704. [PubMed: 3031511]

Mtchedlishvili Z, Bertram EH, Kapur J. Diminished allopreg-nanolone enhancement of GABA(A) receptor currents in a rat model of chronic temporal lobe epilepsy. J Physiol 2001;537:453–465. [PubMed: 11731578]

Naus CC, Bloom FE. Immunohistochemical analysis of the development of somatostatin in the reeler neocortex. Brain Res 1988;471:61–68. [PubMed: 2905929]

Naus CC, Morrison JH, Bloom FE. Development of somatostatin-containing neurons and fibers in the rat hippocampus. Brain Res 1988;468:113–121. [PubMed: 2897870]

Nusser Z, Hajos N, Somogyi P, Mody I. Increased number of GABA-A receptors underlies potentiation of hippocampal synapses. Nature 1998;395:172–177. [PubMed: 9744275]

Obenaus A, Esclapez M, Houser CR. Loss of glutamate decarboxylase mRNA-containing neurons in the rat dentate gyrus following pilocarpine-induced seizures. J Neurosci 1993;13:4470–4485. [PubMed: 8410199]

Otis TS, De Koninck Y, Mody I. Lasting potentiation of inhibition is associated with an increased number of γ-aminobutyric acid type A receptors activated during miniature inhibitory postsynaptic currents. Proc Natl Acad Sci U S A 1994;91:7698–7702. [PubMed: 8052645]

Paxinos, G.; Watson, C. The Rat Brain in the Stereotaxic Coordinates. 4. Academic Press; San Diego, CA: 1998.

Priestley JV, Rethelyi M, Lund PK. Semi-quantitative analysis of somatostatin mRNA distribution in the rat central nervous system using in situ hybridization. J Chem Neuroanat 1991;4:131–153. [PubMed: 1676271]

Ribak CE, Harris AB, Vaughn JE, Roberts E. Inhibitory, GABAergic nerve terminals decrease at sites of focal epilepsy. Science 1979;205:211–214. [PubMed: 109922]

Ribak CE, Bradburne RM, Harris AB. A preferential loss of GABAergic, symmetric synapses in epileptic foci: a quantitative ultrastructural analysis of monkey neocortex. J Neurosci 1982;2:1725–1735. [PubMed: 6815309]

Robbins RJ, Brines ML, Kim JH, Adrian T, de Lanerolle N, Welsh S, Spencer DD. A selective loss of somatostatin in the hippocampus of patients with temporal lobe epilepsy. Ann Neurol 1991;29:325–332. [PubMed: 1675046]

Sayin U, Osting S, Hagen J, Rutecki P, Sutula T. Spontaneous seizures and loss of axo-axonic and axo-somatic inhibition induced by repeated brief seizures in kindled rats. J Neurosci 2003;23:2759–2768. [PubMed: 12684462]

Schmued LC, Hopkins KJ. Fluoro-Jade B: a high affinity fluorescent marker for the localization of neuronal degeneration. Brain Res 2000;874:123–130. [PubMed: 10960596]

Schwarzer C, Williamson JM, Lothman EW, Vezzani A, Sperk G. Somatostatin, neuropeptide Y, neurokinin B and cholecystokinin immunoreactivity in two chronic models of temporal lobe epilepsy. Neuroscience 1995;69:831–845. [PubMed: 8596652]

Seto-Ohshima A, Emson PC, Berchtold MW, Heizmann CW. Localization of parvalbumin mRNA in rat brain by in situ hybridization histochemistry. Exp Brain Res 1989;75:653–658. [PubMed: 2744122]

Shao LR, Dudek FE. Changes in mIPSCs and sIPSCs after kainate treatment: evidence for loss of inhibitory input to dentate granule cells and possible compensatory responses. J Neurophysiol 2005;94:952–960. [PubMed: 15772233]

Sloviter RS. Decreased hippocampal inhibition and a selective loss of interneurons in experimental epilepsy. Science 1987;235:73–76. [PubMed: 2879352]

Sloviter RS. Permanently altered hippocampal structure, excitability, and inhibition after experimental status epilepticus in the rat: the “dormant basket cell” hypothesis and its possible relevance to temporal lobe epilepsy. Hippocampus 1991;1:41–66. [PubMed: 1688284]

Sloviter RS. Possible functional consequences of synaptic reorganization in the dentate gyrus of kainate-treated rats. Neurosci Lett 1992;137:91–96. [PubMed: 1625822]

Sloviter RS, Nilaver G. Immunocytochemical localization of GABA-, cholecystokinin-, vasoactive intestinal polypeptide-, and somatostatin-like immunoreactivity in the area dentata and hippocampus of the rat. J Comp Neurol 1987;256:42–60. [PubMed: 3819038]

Sloviter RS, Dean E, Sollas AL, Goodman JH. Apoptosis and necrosis induced in different hippocampal neuron populations by repetitive perforant path stimulation in the rat. J Comp Neurol 1996;366:516–533. [PubMed: 8907362]

Sloviter RS, Ali-Akbarian L, Horvath KD, Menkens KA. Substance P receptor expression by inhibitory interneurons of the rat hippocampus: enhanced detection using improved immunocytochemical methods for the preservation and colocalization of GABA and other neuronal markers. J Comp Neurol 2001;430:283–305. [PubMed: 11169468]

Sloviter RS, Zappone CA, Harvey BD, Bumanglag AV, Bender RA, Frotscher M. “Dormant basket cell” hypothesis revisited: relative vulnerabilities of dentate gyrus mossy cells and inhibitory interneurons after hippocampal status epilepticus in the rat. J Comp Neurol 2003;459:44–76. [PubMed: 12629666]

Sloviter RS, Zappone CA, Harvey BD, Frotscher M. Kainic acid-induced recurrent mossy fiber innervation of dentate gyrus inhibitory interneurons: possible anatomical substrate of granule cell hyper-inhibition in chronically epileptic rats. J Comp Neurol 2006;494:944–960. [PubMed: 16385488]

Soltesz I, Smetters DK, Mody I. Tonic inhibition originates from synapses close to the soma. Neuron 1995;14:1273–1283. [PubMed: 7605636]

Sun C, Sieghart W, Kapur J. Distribution of alpha1, alpha4, gamma2, and delta subunits of GABAA receptors in hippocampal granule cells. Brain Res 2004;1029:207–216. [PubMed: 15542076]

Tauck DL, Nadler JV. Evidence of functional mossy fiber sprouting in hippocampal formation of kainic acid-treated rats. J Neurosci 1985;5:1016–1022. [PubMed: 3981241]

Tuff LP, Racine RJ, Adamec R. The effects of kindling on GABA-mediated inhibition in the dentate gyrus of the rat. I. Paired-pulse depression. Brain Res 1983;277:79–90. [PubMed: 6315140]

Vezzani A, Schwarzer C, Lothman EW, Williamson J, Sperk. Functional changes in somatostatin and neuropeptide Y containing neurons in the rat hippocampus in chronic models of limbic seizures. Epilepsy Res 1996;26:267–279. [PubMed: 8985706]

Wuarin JP, Dudek FE. Electrographic seizures and new recurrent excitatory circuits in the dentate gyrus of hippocampal slices from kainate-treated epileptic rats. J Neurosci 1996;16:4438–4448. [PubMed: 8699254]

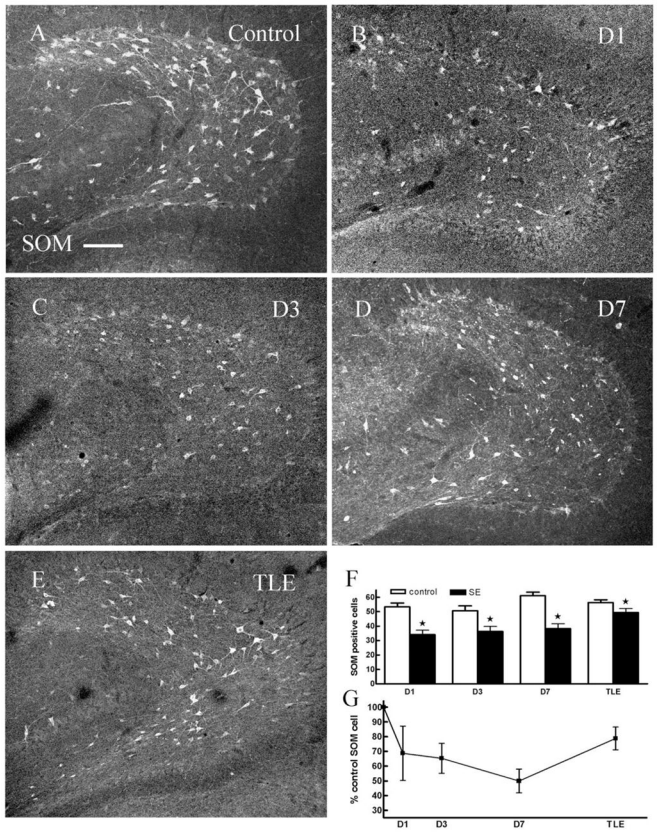

Fig. 1.

There were fewer somatostatin (SOM)-immunoreactive (IR) cells in the dentate hilus in ventral hippocampal sections obtained from animals 1 day (**B**), 3 days (**C**), 7 days (**D**) post-status epilepticus (SE) and in epileptic animals (TLE, **E**) compared to age-matched controls (**A**). **F:** Pairwise comparisons of number of SOM-IR cells in hilus of hippocampi from control and SE-treated animals ($P < 0.05$). **G:** The number of SOM-IR cells in the hilus (expressed as percent controls) in animals 1 day, 3 days, and 7 days following SE and in epileptic animals. D1, 1 day after SE; D3, 3 days after SE; D7, 7 days after SE; TLE, temporal lobe epilepsy. Scale bar = 50 μm.

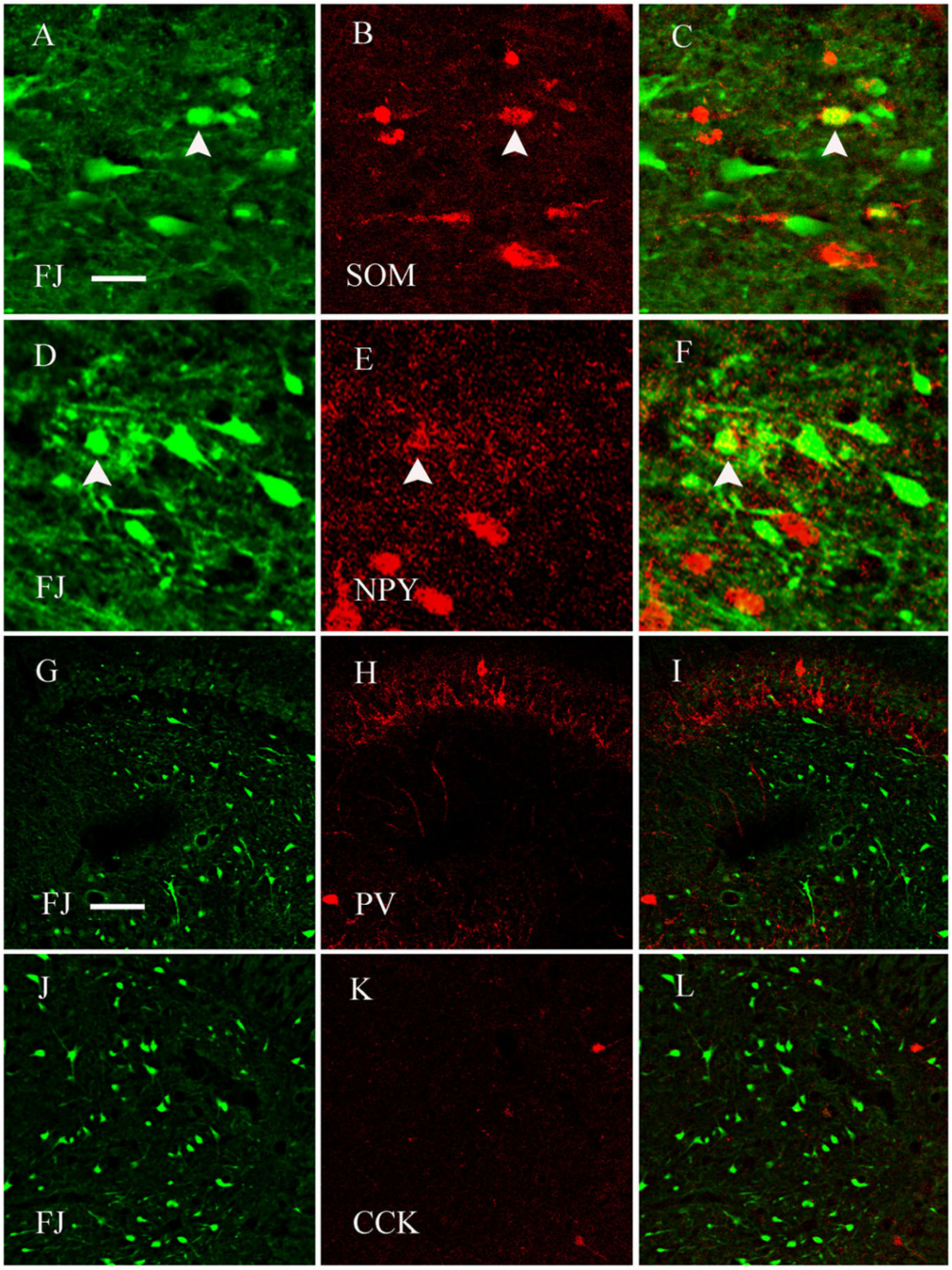

Fig. 2.

Hippocampal sections obtained from animals 24 hours following SE, stained for Fluoro-Jade B and SOM, or neuropeptide Y (NPY), or parvalbumin (PV), or cholecystokinin (CCK). Some SOM and NPY-IR hilar interneurons also stained for Fluoro-Jade B but none of the CCK or PV-IR cells stained for Fluoro-Jade B. **A,D,G,J:** Fluoro-Jade B stained cells in hilus. **B,E,H,K:** SOM, NPY, PV, and CCK-IR cells in the hilus, respectively. **C,F,I,L:** Digitally merged images. Some SOM or NPY-IR interneurons were stained with Fluoro-Jade B also (A–F; arrowhead shows the double-labeled cells). None of the PV and CCK-IR interneurons stained for Fluoro-Jade B. Scale bars = 20 μm in A–F; 50 μm in G–L.

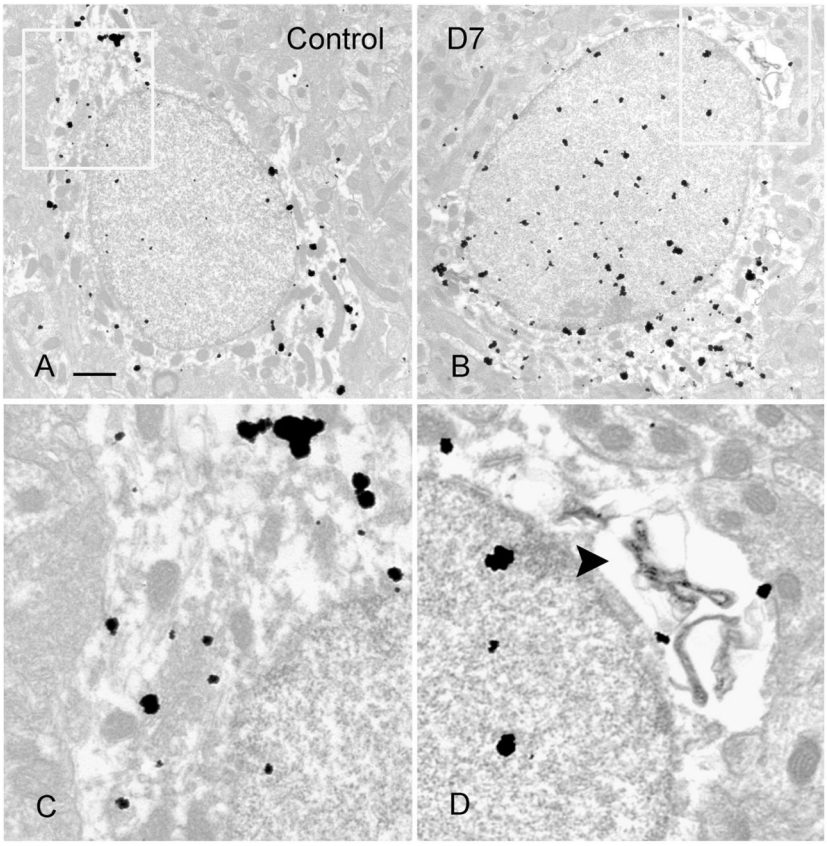

Fig. 3.

Electron micrographs of preembedding silver-enhanced staining of SOM-IR interneurons from hippocampus of a control animal (**A**) and an animal 7 days post-SE (**B**). In B, note perinuclear vacuoles in SOM-IR cell, which is indicative of early degenerative change. Vacuole in boxed area of B was magnified in **D** (arrowhead). Corresponding perinuclear area was boxed in A, magnified in **C**. Scale bar = 1 μm.

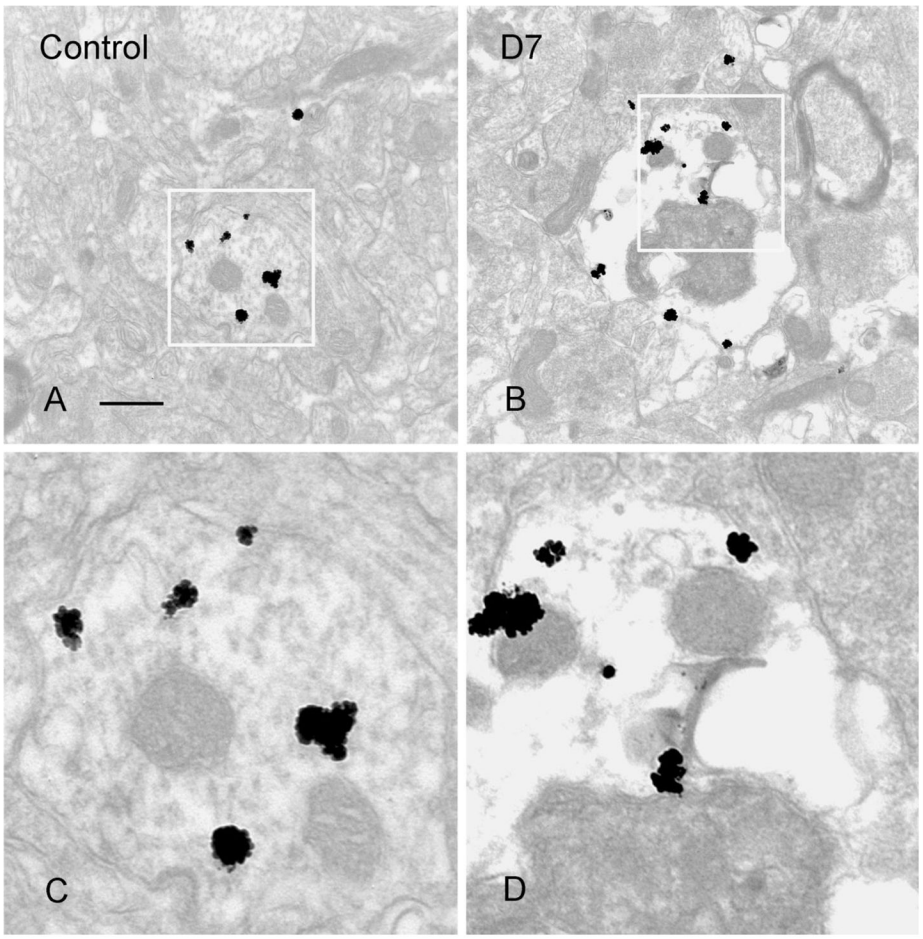

Fig. 4.
Electron micrographs demonstrating a normal SOM-IR dendrite from a control (**A**) and a degenerating dendrite from an animal 7 days post-SE (**B**). Vacuoles and condensation of mitochondria in SOM-IR dendrites were found in B. Boxed areas in A,B are magnified in **C,D**, respectively. Scale bar = 0.5 μm.

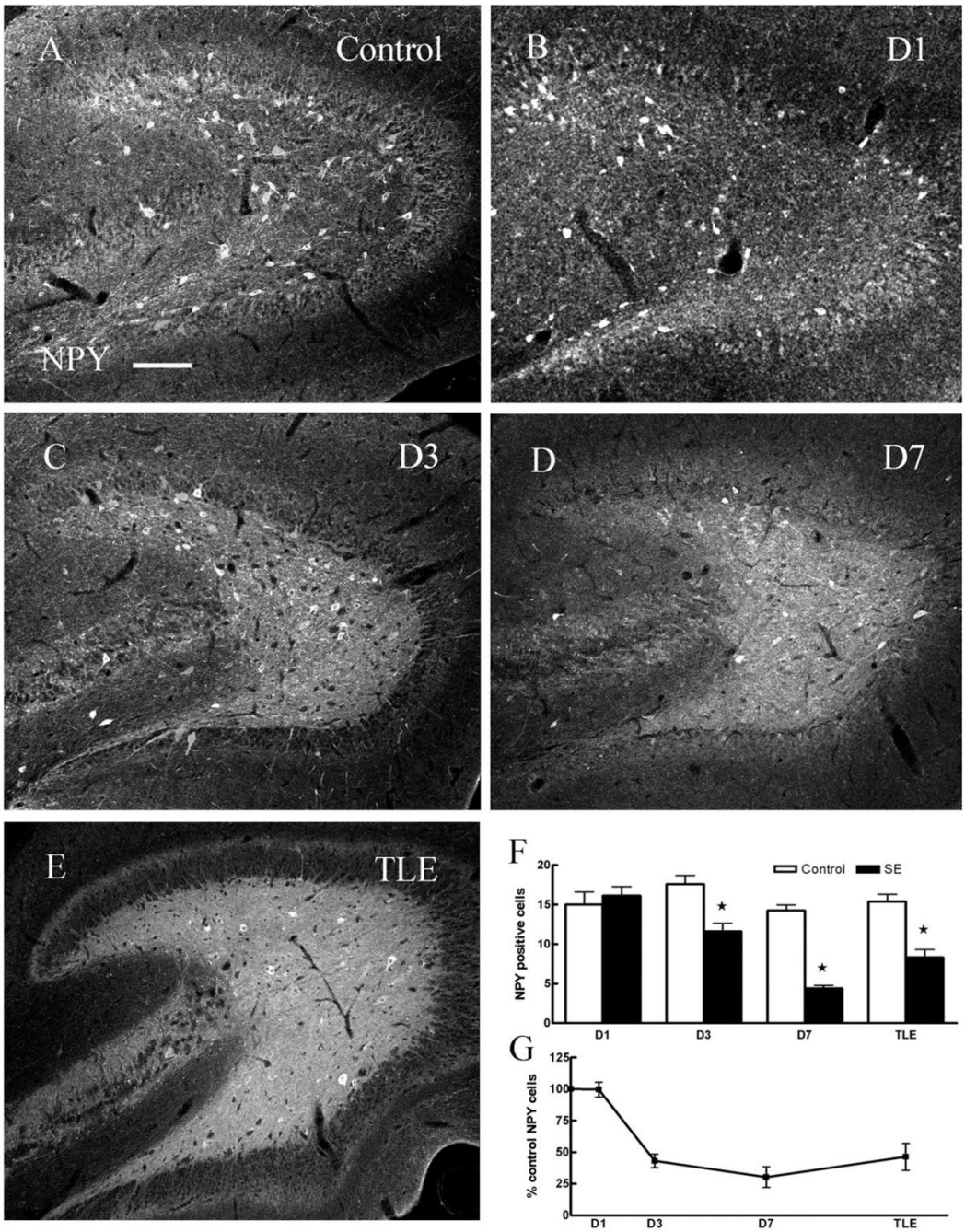

Fig. 5.

There were fewer NPY-IR cells in the dentate hilus in ventral hippocampal sections 3 days (**C**), 7 days (**D**) post-SE, and in TLE (**E**) animals compared to age-matched controls (**A**). **F:** Pairwise comparisons of number of NPY-IR cells in hilus of hippocampi from control and SE-treated animals ($P < 0.05$). **G:** The number of NPY-IR cells in the hilus, expressed as percent controls in animals 1, 3, and 7 days post-SE and in epileptic animals. Scale bar = 50 μm.

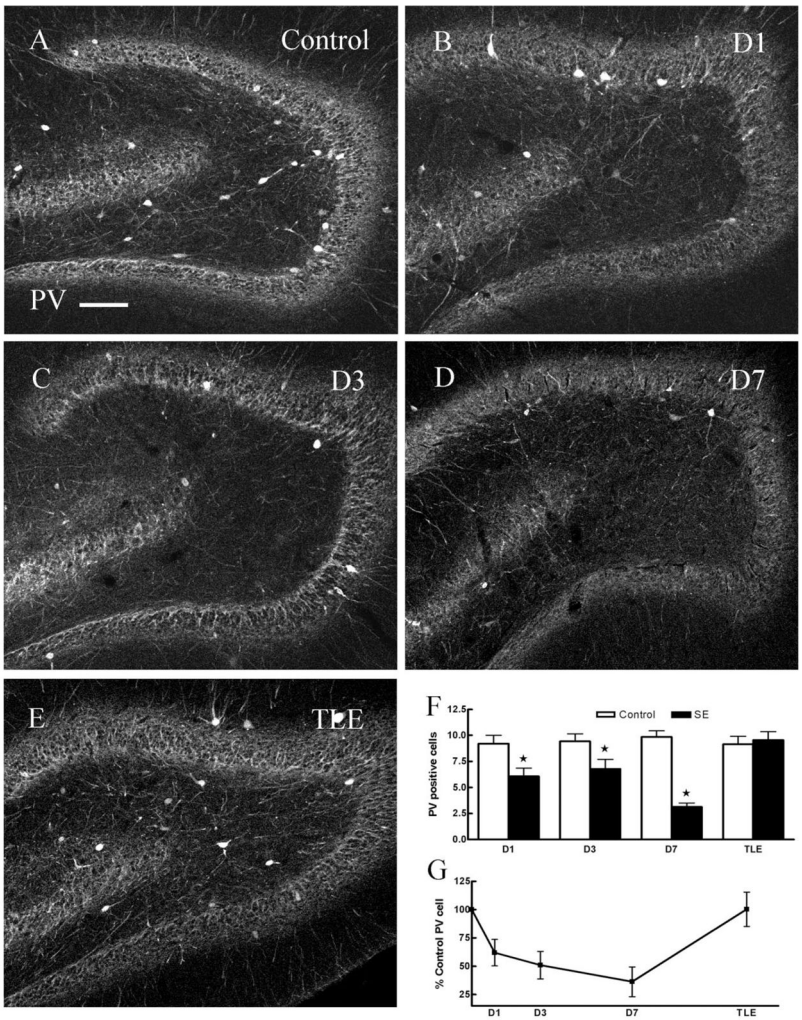

Fig. 6.

Compared to age-matched controls, the number PV-IR cells in the dentate hilus in ventral hippocampal sections 1 day (**B**), 3 days (**C**), 7 days (**D**) post-SE was diminished but was unchanged in epileptic animals (**E**). **F:** Pairwise comparisons of number of PV-IR cells in hilus of hippocampi from control and SE-treated animals (D1, D3, D7, $P < 0.05$; TLE, $P > 0.05$). **G:** The number of PV-IR cells in the hilus (expressed as percent controls) at 1, 3, 7 days post-SE was diminished ($P < 0.05$) and was not changed in TLE animals (E). Scale bar = 50 μm.

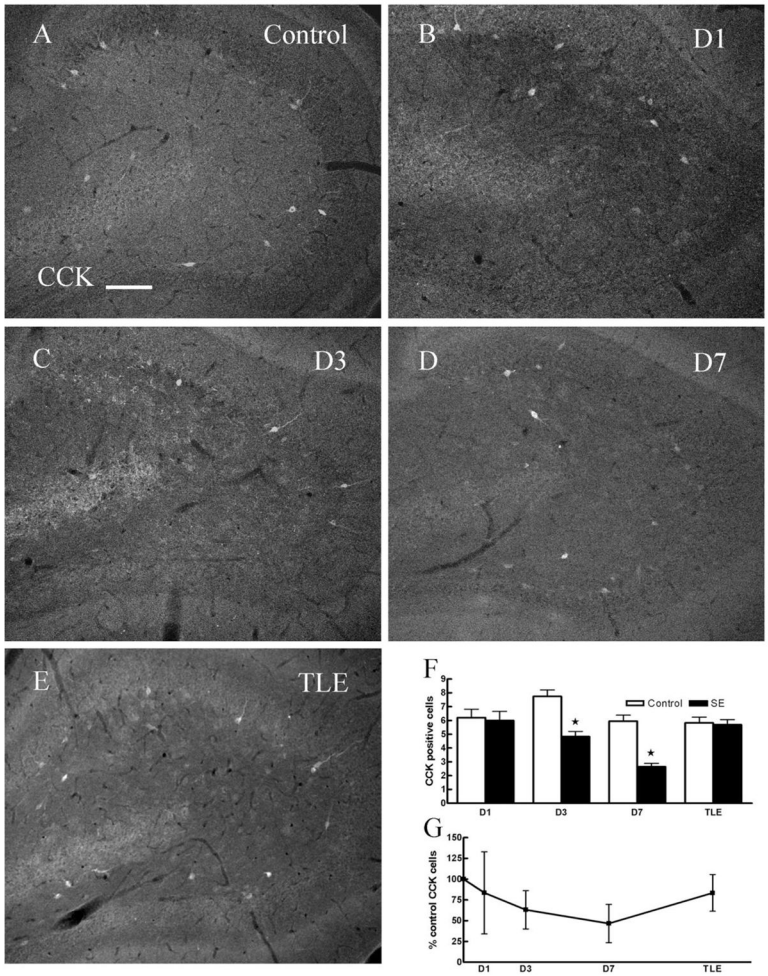

Fig. 7.

Compared to age-matched controls, the number CCK-IR cells in the dentate hilus in ventral hippocampal sections 3 days (**C**), 7 days (**D**) post-SE was diminished but was unchanged in 1 day post-SE (**B**) and epileptic animals (**E**). **F:** Pairwise comparisons of number of CCK-IR cells in hilus of hippocampi from control and SE-treated animals (D3 and D7, $P < 0.05$; D1 and TLE, $P > 0.05$). **G:** The number of CCK-IR cells in the hilus (expressed as percent controls) at 1, 3, 7 days post-SE and in epileptic animals. Scale bar = 50 μm.

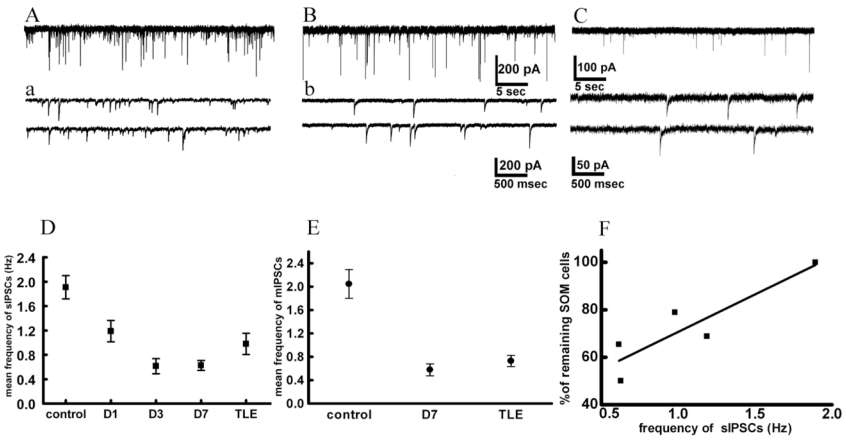

Fig. 8.

Frequency of sIPSCs recorded from DGCs in hippocampal slices from animals 1, 3, and 7 days following SE and from epileptic animals. **A:** Recording from control DGC. **a:** Fragments from the same recording sessions as in A but with a higher temporal resolution. Horizontal scale bars show time; vertical bars show current amplitude in pA. **B,b:** Recording from a DGC from a rat 7 days after SE. **C,c:** Recording from a DGC from a rat with TLE. Note decreased frequency of sIPSCs in TLE. **D:** Mean frequency of sIPSCs decreased progressively after SE and was lowest 7 days post-SE. There was a slight but not significant increase of frequency in TLE compared to day 7. **E:** Frequency of mIPSCs decreased following SE and remained decreased in TLE. Note the similar pattern of frequency decrease of mIPSCs and sIPSCs, suggesting reduction in number of release sites. Each point represents mean Hz ± SEM. **F:** Correlation between decrease in number of SOM-IR cells and reduction of frequency of sIPSCs after SE. Abscissa shows number of SOM-IR cells is shown as percentage of surviving cells where 100% is taken as a control. Ordinate shows frequency of sIPSCs in Hz. Each point represents time after SE.

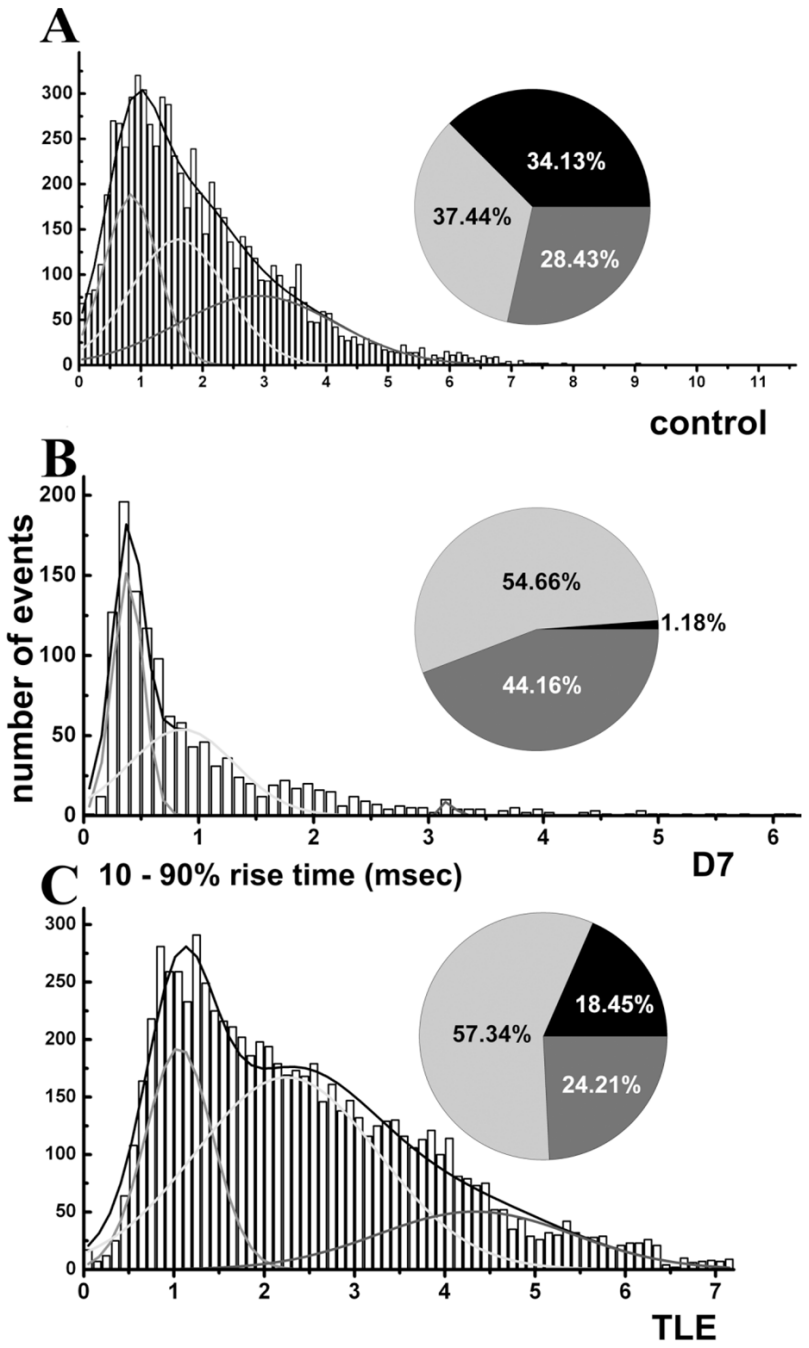

Fig. 9.

Frequency distribution histograms of 10 –90% rise times of mIPSCs recorded from DGC from a control (**A**), 7 days post-SE (**B**) and in TLE (**C**) animals. Approximately 7,500 mIPSCs from 5– 6 cells were pooled in control and TLE groups. Approximately 1,300 events were pooled from four DGCs in animals 7 days post-SE. Rise times were binned to 0.1-ms bin size and fit to multiple Gaussian distributions. Curves show fast (light gray), intermediate (black), and slow (dark gray) rise time distributions. Proportions of the events in three populations are displayed in corresponding pie charts where light gray, black, and dark gray segments correspond to fast, intermediate, and slow rise times. Note that slow rise time events were

markedly diminished 7 days post-SE. There was a reduction of proportion of slow rise time events and an increase of proportion of intermediate events in TLE compared to control.

TABLE 1

Average Neuropeptide-Containing Interneurons per Section

		SOM		NPY		PV		CCK	
		Mean ± SEM	**N**	**Mean ± SEM**	**N**	**Mean ± SEM**	**N**	**Mean ± SEM**	**N**
D1	Post-SE	34 ± 3.0**	33	16 ± 1.5	36	6 ± 0.8*	24	6 ± 0.7	26
	Control	53 ± 2.7	44	15 ± 1.6	18	9 ± 0.8	35	6 ± 0.6	40
D3	Post-SE	36 ± 3.5*	31	12 ± 1.0**	34	7 ± 0.9*	35	5 ± 0.4**	35
	Control	51 ± 3.4	23	18 ± 1.1	36	9 ± 0.7	36	8 ± 0.5	23
D7	Post-SE	38 ± 3.4**	39	5 ± 0.4**	35	3 ± 0.4**	35	3 ± 0.2**	45
	Control	61 ± 2.5	32	14 ± 0.7	34	10 ± 0.6	34	6 ± 0.4	35
TLE	Epileptic	49 ± 2.7*	40	8 ± 1.0*	47	10 ± 0.8	46	6 ± 0.4	48
	Control	56 ± 1.9	46	15 ± 0.9	60	9 ± 0.8	61	6 ± 0.4	51

See list for abbreviations.

*$P < 0.05$,

**$P < 0.001$,

N is the number of sections.